UNIVERSITY
OF TRENTO

DEPARTMENT OF INFORMATION AND COMMUNICATION TECHNOLOGY

38050 Povo – Trento (Italy), Via Sommarive 14
http://www.dit.unitn.it

AN INNOVATIVE FUZZY-LOGIC-BASED STRATEGY FOR AN EFFECTIVE EXPLOITATION OF NOISY INVERSE SCATTERING DATA

Renzo Azaro, Aronne Casagranda, Davide Franceschini, and Andrea Massa

October 2004

Technical Report DIT-04-097

An Innovative Fuzzy-Logic-Based Strategy for an Effective Exploitation of Noisy Inverse Scattering Data

Renzo Azaro, Aronne Casagranda, Davide Franceschini, and Andrea Massa

Department of Information and Communication Technologies,

University of Trento, Via Sommarive 14, I-38050 Trento - Italy

Tel. +39 0461 882057, Fax +39 0461 882093

E-mail: *andrea.massa@ing.unitn.it*,

{*renzo.azaro, aronne.casagranda, davide.franceschini*}*@dit.unitn.it*

Web-page: *http://www.eledia.ing.unitn.it*

An Innovative Fuzzy-Logic-Based Strategy for an Effective Exploitation of Noisy Inverse Scattering Data

Renzo Azaro, Aronne Casagranda, Davide Franceschini, and Andrea Massa

Abstract

This paper presents an innovative inverse scattering approach based on a fuzzy-logic strategy aimed at fully exploiting the information content of the scattered data in a microwave imaging system. The effectiveness of the proposed method is assessed through the results of a numerical analysis concerned with the reconstruction of single as well as multiple dielectric targets in various noisy environments. For comparison purposes, the obtained performance are compared with those of a standard method in terms of reconstruction accuracy and computational load to point out the improvement induced by the proposed approach.

Key words:

Microwave Imaging, Inverse Scattering, Fuzzy-Logic.

1 Introduction

Microwave imaging is a technique aimed at investigating and reconstructing the electromagnetic properties of an inaccessible area (for a general overview see [1], [2], [3] and the reference therein). Towards this aim, the investigation domain is probed by means of a set of incident electromagnetic fields and the scattering interactions with the structure under test are detected through a set of sensors placed outside the inaccessible area.

In such a framework, the collection of the scattering information is a key point of the imaging process, but severe obstacles prevent the acquisition of a completely reliable set of measurements since unavoidable sources of error operate. For instance, the electromagnetic interferences contribute to the corruption of the data together with systematic errors caused by the inaccurate mechanical positioning of experimental acquisition arrangement. The impact of such "*disturbances*" is further emphasized by the intrinsic instability of every inverse scattering problem [4]. To limit such effects, the retrieval problem is usually regularized by defining a suitable cost function and searching for the estimation of the scenario under test that best matches the available scattering data. Although such a countermeasure circumscribes the ill-conditioning, the presence of noise could lead the reconstruction algorithm towards a false solution. To avoid this event, a reliable estimation of the information content in the measured data (i.e., distinguishing between the contribute of the scattering and of the noise in the measured data) is very appealing.

Since a "*direct*" evaluation would be complex and very expensive from an experimental point of view, the authors propose in this work an unsupervised technique. Towards this aim, the potentialities of a *fuzzy-logic* [5] based strategy are exploited in the retrieval process to obtain a *degree of reliability* of each noisy measure.

The paper is organized as follows. In Sect. 2, the *fuzzy-logic* system is described then the results of a preliminary assessment are presented and analyzed by considering a selected set of synthetic scenarios (Sect. 3). Finally, some conclusions are drawn (Sect. 4).

2 Mathematical Formulation and Fuzzy-Logic Based Approach

Let us consider a two-dimensional geometry where an investigation domain D_{inv} is illuminated by a set of V known incident fields ($\mathbf{E}_v^{inc}(\mathbf{r}) = E_v^{inc}(x,y)\hat{\mathbf{z}},\ v = 1,...,V$) to determine its electromagnetic characteristics modeled in terms of the object function $\tau(x,y) = [\varepsilon_r(x,y) - 1] - j\frac{\sigma(x,y)}{2\pi f}$, $\varepsilon_r(x,y)$ and $\sigma(x,y)$ being the relative dielectric permittivity and the electric conductivity, respectively; f is the working frequency. Such an imaging process is carried out starting from the scattered field collected in an observation domain D_{obs} external to D_{inv}.

The physical relationship between the object function $\tau(x,y)$ and the field scattered in the observation domain, $L_{D_{obs}}(x_m,y_m)$, $(x_m,y_m) \in D_{obs}$, is mathematically described by mans of the *Integral Data Equation* [6]

$$L^v_{D_{obs}}(x_m,y_m) = k^2 \int_{D_{inv}} G^{ext}(x_m,y_m|x',y')\tau(x',y')E_v^{tot}(x',y')dx'dy' \quad (x_m,y_m) \in D_{obs} \tag{1}$$

where $G(x,y \mid x',y') = -\frac{j}{4}H_0^{(2)}\left(k_0\sqrt{(x-x')^2+(y-y')^2}\right)$, k being the free-space wavenumber, and $H_0^{(2)}$is the Hankel function of 0-*th* order and second kind; $E_v^{tot}(x,y)$ is the electric field corresponding to the v-*th* illumination.

Moreover, the scattering phenomena in D_{inv} can be suitably represented in terms of the *Integral State Equation* [6]

$$L^v_{D_{inv}}(x_n,y_n) = E_v^{tot}(x_n,y_n) - k^2 \int_{D_{inv}} G^{int}(x_n,y_n \mid x',y')\tau(x',y')E_v^{tot}(x',y')dx'dy' \quad (x_n,y_n) \in D_{inv} \tag{2}$$

In order to reconstruct $\tau(x,y)$ and $E_v^{tot}(x,y)$ in the investigation domain, preventing the ill-posedness of the problem, a widely adopted technique consists in defining a suitable cost function [7] proportional to the fitting between measured and reconstructed scattering data

$$\Phi\left\{\tau(x_n,y_n),\ E_v^{tot}(x_n,y_n)\right\} = \Phi_{Data}\left\{\tau(x_n,y_n),\ E_v^{tot}(x_n,y_n)\right\} + \Phi_{State}\left\{\tau(x_n,y_n),\ E_v^{tot}(x_n,y_n)\right\}$$
$$n = 1,...,N \qquad v = 1,...,V \tag{3}$$

$$\Phi_{Data}\left\{\tau(x_n,y_n),\ E_v^{tot}(x_n,y_n)\right\} = \frac{\sum_{v=1}^{V}\sum_{m=1}^{M}\left\{\gamma_v^m\left|E_v^{scatt}(x_m,y_m) - L_{D_{obs}}^v(x_m,y_m)\right|^2\right\}}{\sum_{v=1}^{V}\sum_{m=1}^{M}\left\{\left|E_v^{scatt}(x_m,y_m)\right|^2\right\}} \qquad (Data\ Term) \tag{4}$$

$$\Phi_{State}\left\{\tau(x_n,y_n),\ E_v^{tot}(x_n,y_n)\right\} = \frac{\sum_{v=1}^{V}\sum_{n=1}^{N}\left\{\Psi_v^n\left|E_v^{inc}(x_n,y_n) - L_{D_{inv}}^v(x_n,y_n)\right|^2\right\}}{\sum_{v=1}^{V}\sum_{n=1}^{N}\left\{\left|E_v^{inc}(x_n,y_n)\right|^2\right\}} \qquad (State\ Term) \tag{5}$$

M (or N) being the numbers of positions in D_{obs} (or in D_{inv}) where the scattered field (or the incident field) is collected. γ_v^m and Ψ_v^n are reliability coefficients for $L_{D_{obs}}^v(x_m,y_m)$ and $L_{D_{inv}}^v(x_n,y_n)$, respectively, which allow to take into account the presence of noise in the collected data. Such reliability indexes are computed in an unsupervised way by means of the fuzzy-logic system shown in Fig. 1.

More in detail, the inputs of the *fuzzifier* (the first block in Fig. 1) are two sequences (ν_m^v and υ_n^v) concerning the collected data according to the following expressions

$$\nu_m^v = \frac{\left|\frac{E_v^{scatt}(x_m,y_m)}{E_v^{tot}(x_m,y_m)}\right|}{max_v\left\{max_m\left|\frac{E_v^{scatt}(x_m,y_m)}{E_v^{tot}(x_m,y_m)}\right|\right\}}, \qquad \upsilon_v^n = \frac{\left|E_v^{inc}(x_n,y_n)\right|}{max_v\left\{max_n\left|E_v^{inc}(x_n,y_n)\right|\right\}} \qquad \begin{matrix} v = 1,...,V \\ m = 1,...,M \\ n = 1,...,N \end{matrix} \tag{6}$$

. Then, a fuzzy counterpart, represented by a Gaussian membership function $g(\nu_m^v)$ [or $g(\upsilon_m^v)$] [5] centered in ν_m^v (or υ_m^v) and characterized by a variance $\chi = 10^{-4}$, is associated to each input value of the fuzzifier. The membership function interacts with an *a-priori* heuristically-defined *"Dataset of Rules"* composed by a set of *Antecedents* and related *Consequences* [Fig. 2(a)]. During the *fuzzy inference* phase, the system determines an activation value $\mu(\nu_m^v)$ [or $\mu(\upsilon_m^v)$] for each *Antecedent*, obtained by computing the intersection between $g(\nu_m^v)$ [or $g(\upsilon_m^v)$] and the *Antecedent* itself.

As far as the "*Rule 4*" is concerned, such a procedure is shown on the left side of Fig. 2(a). The same figure displays the definition of the *"degree of truth"* of the associated

Consequence ("Cons4") starting from the activation value.

The process is repeated for each rule (i.e., for each couple of *Antecedent-Consequence*) to obtain the composition of the final degree of truth as indicated in Fig. $2(b)$ by the shadowed region (called "*truth region*").

The last step (called *defuzzification*) of the unsupervised data-processing consists in computing the reliability index γ_v^m (or Ψ_v^n), which is defined as the center of the truth region [Fig. $2(b)$].

Successively, starting from such a set of coefficients (γ_v^m, Ψ_v^n; $n = 1, ..., N$, $m = 1, ..., M$, $v = 1, ..., V$), whatever reconstruction algorithm is used to minimize the arising cost function (3), it could usefully exploit the scattering data according to their degree of reliability.

3 Numerical Results

In this Section, a selected set of numerical results will be shown to give some indications on the improvement over a standard approach when pre-processing the input data by means of the fuzzy-system. Such results will be concerned with three different scattering scenarios depicted in Fig. 3[(1)]. They refer to scatterers located in a square investigation domain of side λ_0 (λ_0 being the free-space wavelength) probed by a set of monochromatic plane waves and partitioned in $N = 225$ equal square sub-domains according to the Richmond's procedure [8]. The "*Test Case 1*" consists of a square $\frac{\lambda_0}{5}$-sided homogeneous ($\tau = 1.5$) cylinder sensed by $V = 4$ different directions ($\theta_{inc}^v = \frac{2\pi}{V}(v-1)$, $v = 1, ..., V$), while in the second one (*Test Case 2*) is a similar profile but larger ($L = \frac{\lambda_0}{3}$ in side) and probed with $V = 8$ different incident fields. In the "*Test Case 3*", two scatterers are located $d = \frac{\lambda_0}{3}$ far the one from the other ($L_1 = L_2 = \frac{\lambda_0}{5}$ and $\tau_1 = \tau_2 = 1.5$). The scattering data have been numerically computed in $M = 10$ sampling points by adding a random Gaussian noise with a fixed signal-to-noise ratio (SNR) to simulate realistic

[(1)] Please note that the black pixel in the lower right border of the image is used for reference.

environmental conditions.

As far as the minimization procedure is concerned, since the focus is on the comparison between the fuzzy-logic-based technique and the reference one (the "*bare*" approach), a simple iterative conjugate-gradient optimizer [9] has been used. Our more recent advances on the minimization of the inverse scattering cost function have been described elsewhere [10] and it will be used in the near future to fully exploit the effectiveness of an integrated strategy based on the fuzzy-logic data processing.

In order to quantitatively estimate the improvement in the *quantitative imaging* allowed by the fuzzy-logic-based processing, the following error figures are defined

$$\zeta_j = \frac{1}{N^{(j)}} \sum_{n=1}^{N^{(j)}} \left\{ \frac{\tau(x_n, y_n) - \tau^{ref}(x_n, y_n)}{\tau^{ref}(x_n, y_n)} \right\} \times 100 \tag{7}$$

where $N^{(j)}$ ranges over the whole investigation domain ($N^{(j)} = N$, $j \Rightarrow tot$), or over the area occupied by the actual scatter ($j \Rightarrow int$), or over the background ($j \Rightarrow ext$).

Then, let us analyze the results of the numerical assessment starting from the first experiment. As expected, the fuzzy-logic data processing, acting before the minimization process, significantly impacts when $SNR \leq 20dB$, that is in those situations where the measured data are seriously corrupted by the noise. Such an event can be noticed in Figs. $4(a)$-(c) where it is pointed out that the fuzzy-based strategy achieves smaller values of the error figures[(2)] than those of the standard method. Pictorially, such an improvement can be appreciated by comparing the images of the reconstructed contrasts when $SNR = 10\,dB$ [Fig. $5(a)$ vs. Fig. $5(b)$] and $SNR = 5dB$ [Fig. $5(c)$ vs. Fig. $5(d)$]. Such a behavior is due to the better fitting with the scattering data allowed by the proposed methodology.

In fact, the minimization of the cost function benefits of the action of the reliability coefficients γ_v^m and Ψ_v^n as shown in Fig. 6 where two representative samples of the behavior

[(2)] Because of the statistical nature of the noise, each situation characterized by a different SNR has been executed several times to assess the quality of the solution. Therefore, the reported results are the averages of the execution of the imaging process for 50 independent realizations of the data-generation process given a fixed value of the signal-to-noise ratio.

of the cost function during the iterative minimization are given [Fig. 6(a) - $SNR = 10\,dB$; Fig. 6(b) - $SNR = 5dB$]. As can be observed, the total number of iterations needed to reach the convergence ($\Phi^{(k)} \leq \eta$, $\eta = 10^{-3}$; k being the iteration index) or a stationary condition ($\frac{\left|K_{window}\Phi^{(k)} - \sum_{h=1}^{K_{window}} \Phi^{(h)}\right|}{\Phi^{(k)}} \leq \gamma_{st}$, $K_{window} = 20$ and $\gamma_{st} = 10^{-2}$). Moreover, as far as the standard approach is concerned, such a number increases and the rate of convergence reduces when the noise level grows, while it keeps an almost constant value (~ 700) when the fuzzy-based strategy is adopted.

This behavior is also pointed out in Fig. 7 where the mean values of the total number of iteration needed to minimize the cost function is reported. Such a value turns out to be more insensitive to the SNR value when the new method is applied. On the contrary, large variations occur when the reference approach is used.

Similar conclusions, in terms of convergence rate and reconstruction accuracy, hold true for the *Test Case 2* (Fig. 8) and the multiple-scatterers configuration (*Test Case 3* - Fig. 9). As far as the two-objects configuration is concerned, the obtained results confirm the effectiveness of the fuzzy-based approach in dealing with complex scenarios, as well. According to the indications carried out from the behaviors of the error figures in Fig. 9, the reconstructed profiles [Figs. 10(b)-(c)] better approximate the actual ones and the presence of artifacts in the final image is avoided.

For completeness, Figure 11 shows the plots of the cost function for a realization of the reconstruction process when $SNR = 10\,dB$ and $SNR = 5\,dB$, respectively.

4 Conclusions

In this paper, an innovative fuzzy-logic-based methodology aimed at exploiting the information content of noisy data by means of an unsupervised procedure has been presented. Such a strategy allows to take into account the reliability of the measurements through a set of weighting coefficients in the cost function to be minimized. The effectiveness of the proposed approach has been analyzed by means of some synthetic experiments

concerning various scattering configurations as well as noisy environments. The achieved results have shown a noticeable reduction of the required computational load as well as an improvement in the reconstruction of the scenario under test.

Acknowledgments

The authors wish to express their gratitude to E. Vico for helpful discussions on the paper.

References

[1] J. C. Bolomey, "Microwave diffraction tomography for biomedical applications," *IEEE Trans. Microwave Theory Tech.*, vol. 30, pp. 1998-2000, 1982.

[2] J. C. Bolomey, "Recent European developments in active microwave for industrial, scientific and medical applications," *IEEE Trans. Microwave Theory Tech.*, vol. 37, pp. 2109-2117, 1989.

[3] J. Ch. Bolomey. *Frontiers in Industrial Process Tomography.* Engineering Foundation, 1995.

[4] D. Colton and R. Kress, Inverse Acoustic and Electromagnetic Scattering Theory. Springer, Berlin, 1992

[5] L. A. Zadeh, "Fuzzy Sets," *Information and Control*, vol. 8, pp. 338-353, 1965.

[6] D. S. Jones, *The Theory of Electromagnetism.* Oxford, U.K.: Pergamon Press, 1964.

[7] R. E. Kleinman and P. M. Van den Berg, "A modified gradient method for two-dimensional problems in tomography," *J. Comput. Appl. Math.*, vol. 42, pp. 17-35, 1992.

[8] J. H. Richmond, "Scattering by a dielectric cylinder of arbitrary cross section shape," *IEEE Trans. Antennas Propagat.*, vol. 13, pp. 334-341, 1965.

[9] R. V. Kohn and A. McKenney, "Numerical implementation of a variational method for electrical impedance tomography," *Inverse Problems*, vol. 6, pp. 389-414, 1990.

[10] S. Caorsi, M. Donelli, A. Lommi, and A. Massa, "Location and imaging of two-dimensional scatterers by using a particle swarm algorithm," *J. Electrom. Waves Appl.*, vol. 18, pp. 481-494, 2004.

FIGURE CAPTIONS

- **Figure 1.**

  Block-diagram of the fuzzy system.

- **Figure 2.**

  Dataset of Rules employed for processing the input data of the fuzzy system.

- **Figure 3.**

  Numerical validation - Actual profiles: (a) *Test Case 1*, (b) *Test Case 2*, and (c) *Test Case 3*.

- **Figure 4.**

  Test Case 1 - Average values of the error figures versus SNRs: (a) total error ζ_{tot}, (b) internal error ζ_{int}, and (c) external error ζ_{ext}.

- **Figure 5.**

  Test Case 1 - Samples of the dielectric profiles reconstructed by using the standard approach (a)-(c) and the fuzzy-logic-based strategy (b)-(d) when $SNR = 10\,dB$ (a)-(b) and $SNR = 5\,dB$ (c)-(d).

- **Figure 6.**

  Test Case 1 - Behavior of the cost function during the minimization process when (a) $SNR = 10\,dB$ and (b) $SNR = 5\,dB$.

- **Figure 7.**

  Test Case 1 - Average number of iterations needed to reach the convergence versus the signal-to-noise ratio.

- **Figure 8.**

  Test Case 2 - Average values of the error figures versus SNRs: (a) total error ζ_{tot}, (b) internal error ζ_{int}, and (c) external error ζ_{ext}.

- **Figure 9.**

  Test Case 3 - Average values of the error figures versus SNRs: (a) total error ζ_{tot}, (b) internal error ζ_{int}, and (c) external error ζ_{ext}.

- **Figure 10.**

  Test Case 3 - Samples of the dielectric profiles reconstructed by using the standard approach (a)-(c) and the fuzzy-logic-based strategy (b)-(d) when $SNR = 10\,dB$ (a)-(b) and $SNR = 5\,dB$ (c)-(d).

- **Figure 11.**

  Test Case 3 - Behavior of the cost function during the minimization process when (a) $SNR = 10\,dB$ and (b) $SNR = 5\,dB$.

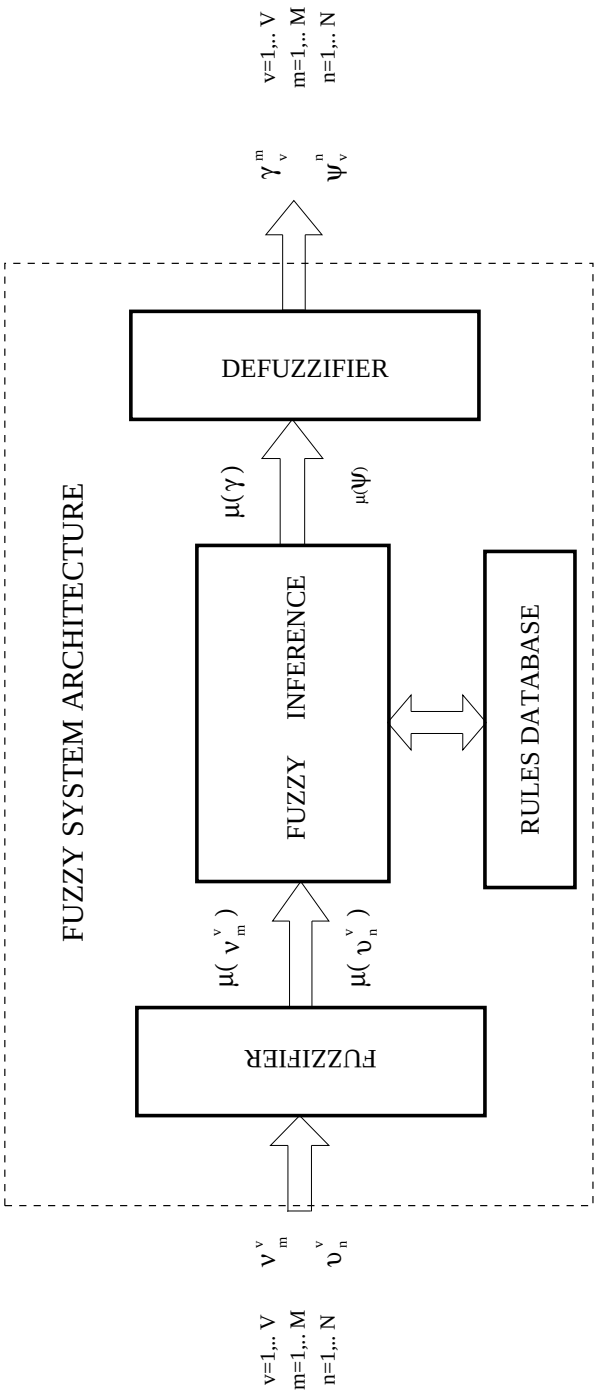

Fig. 1 - R. Azaro *et al.*, "An Innovative Fuzzy-Logic-Based Strategy ..."

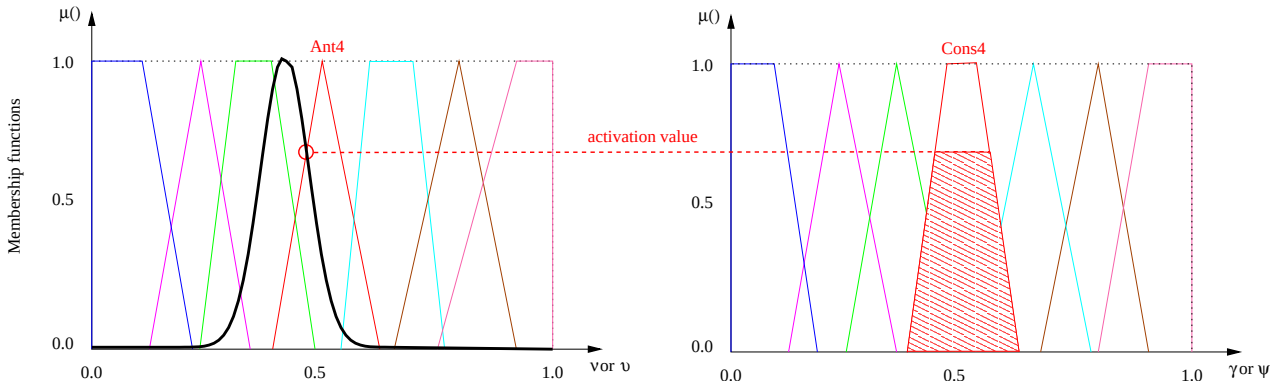

(*a*)

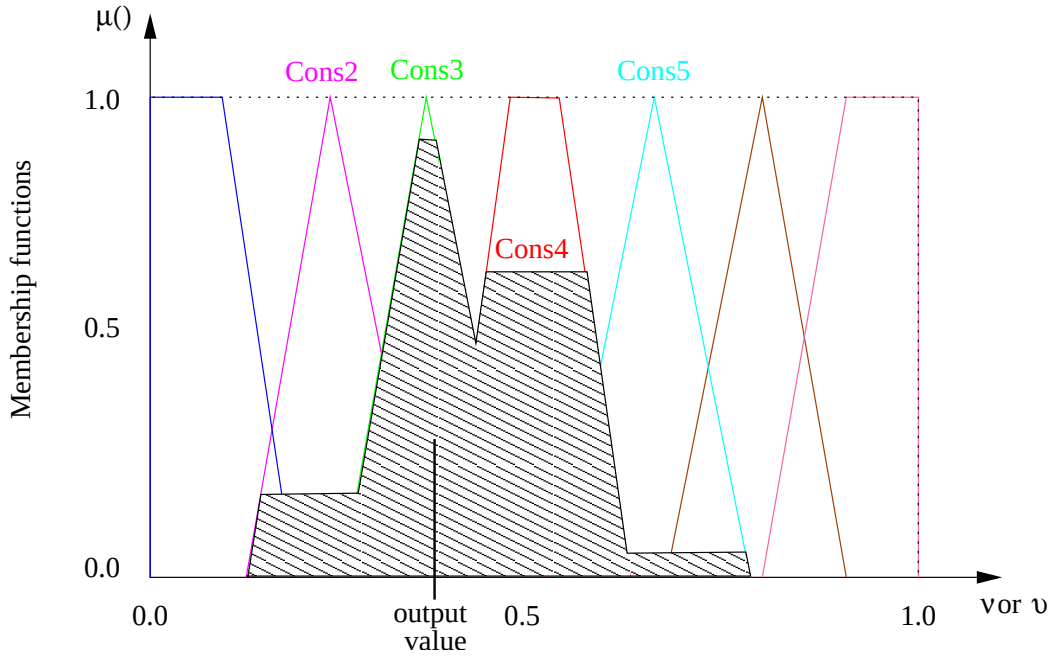

(*b*)

Fig. 2 - R. Azaro *et al.*, "An Innovative Fuzzy-Logic-Based Strategy ..."

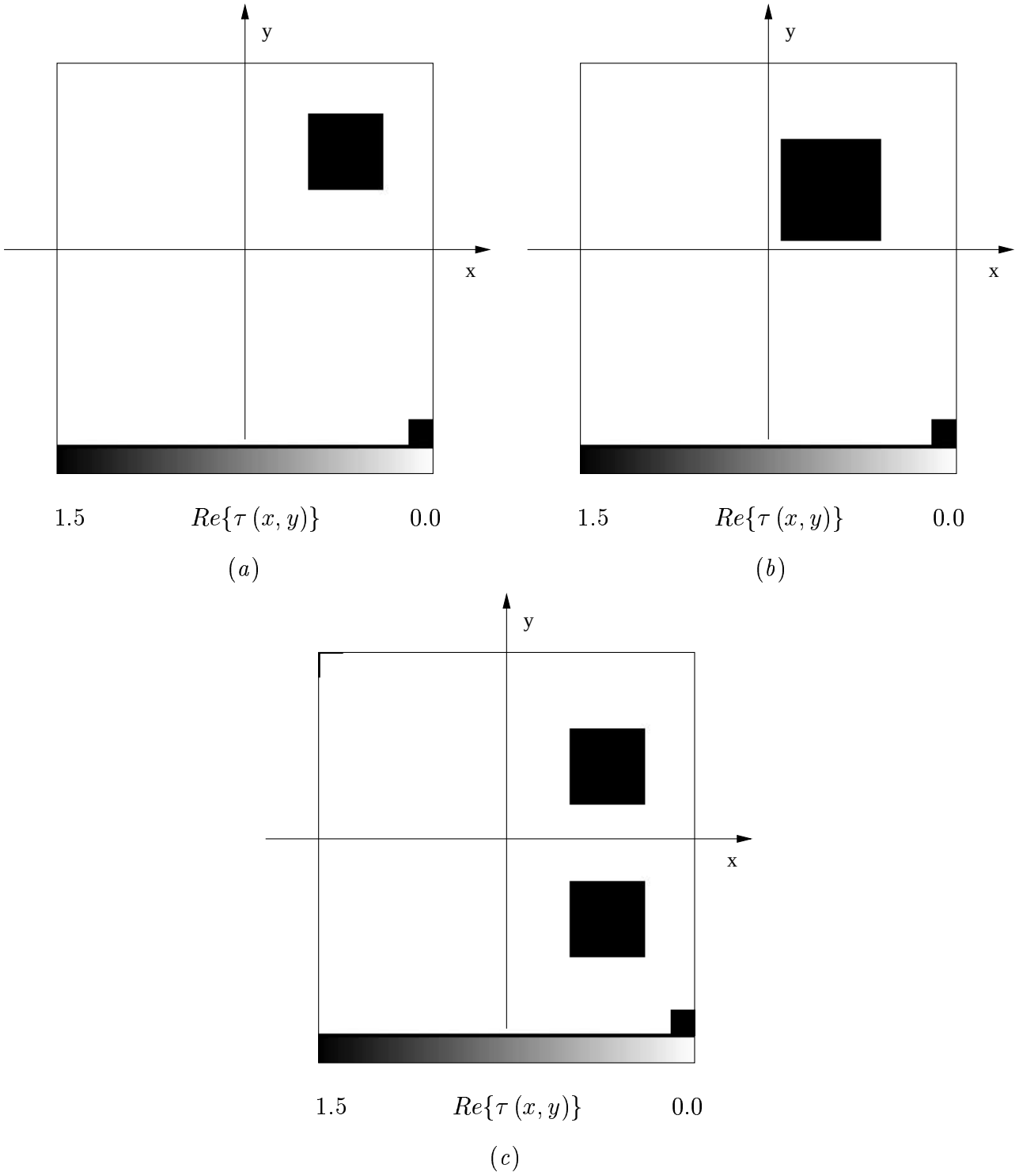

Fig. 3 - R. Azaro *et al.*, "An Innovative Fuzzy-Logic-Based Strategy ..."

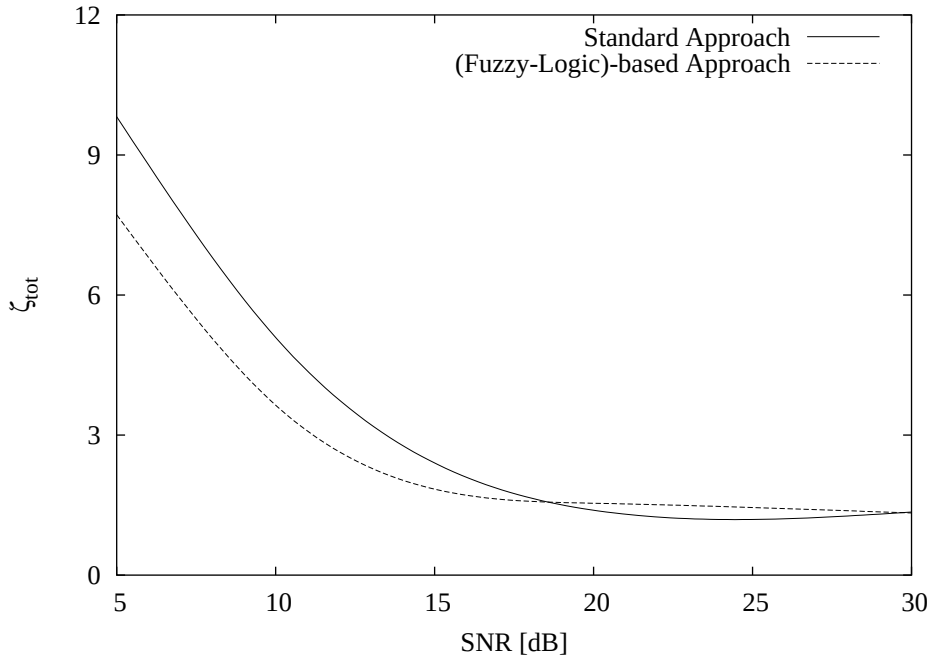

(a)

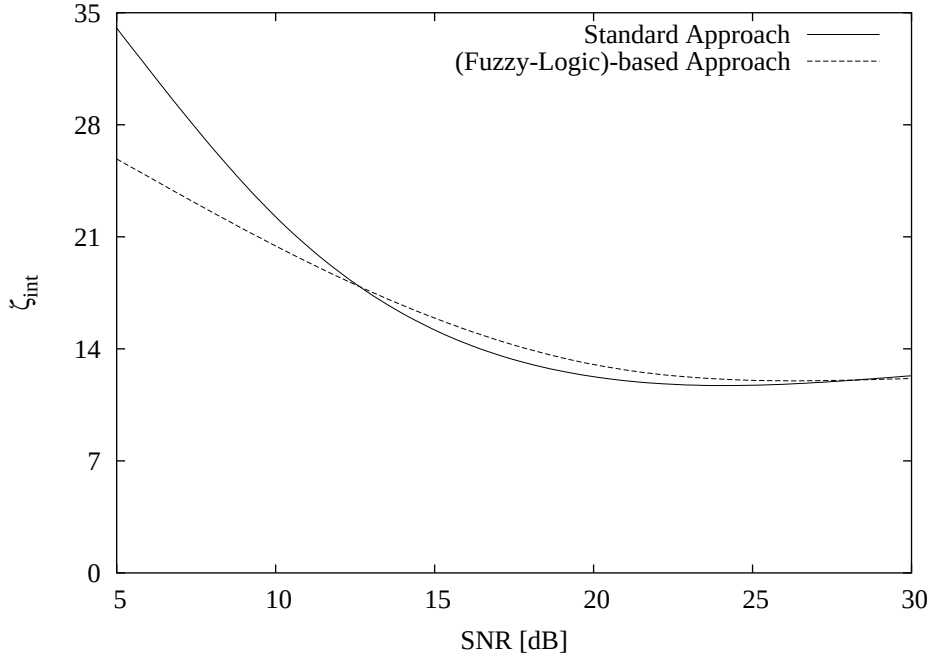

(b)

Fig. 4(I) - R. Azaro *et al.*, "An Innovative Fuzzy-Logic-Based Strategy ..."

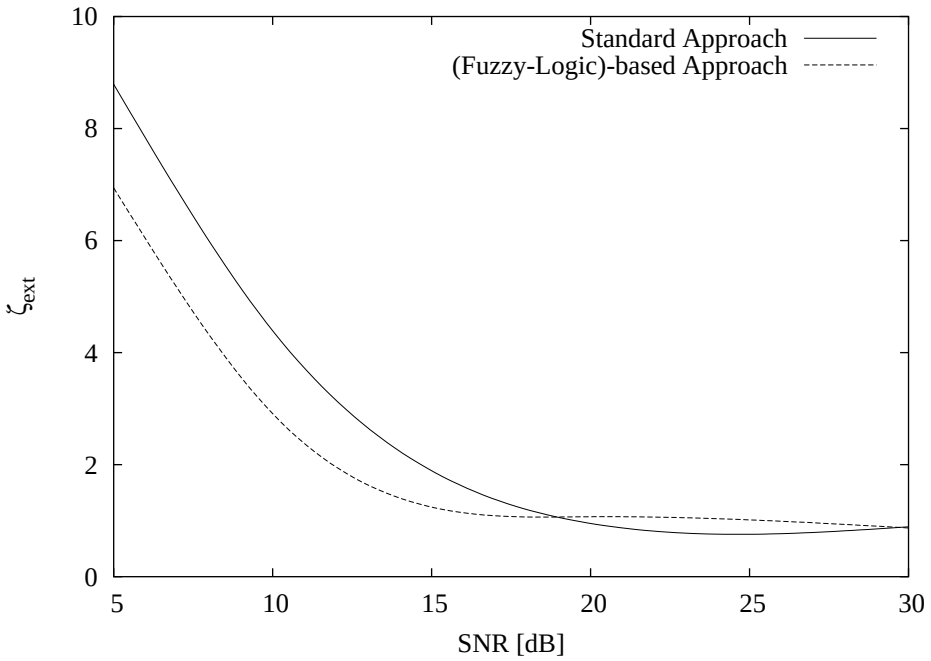

(c)

Fig. 4(*II*) - R. Azaro *et al.*, "An Innovative Fuzzy-Logic-Based Strategy ..."

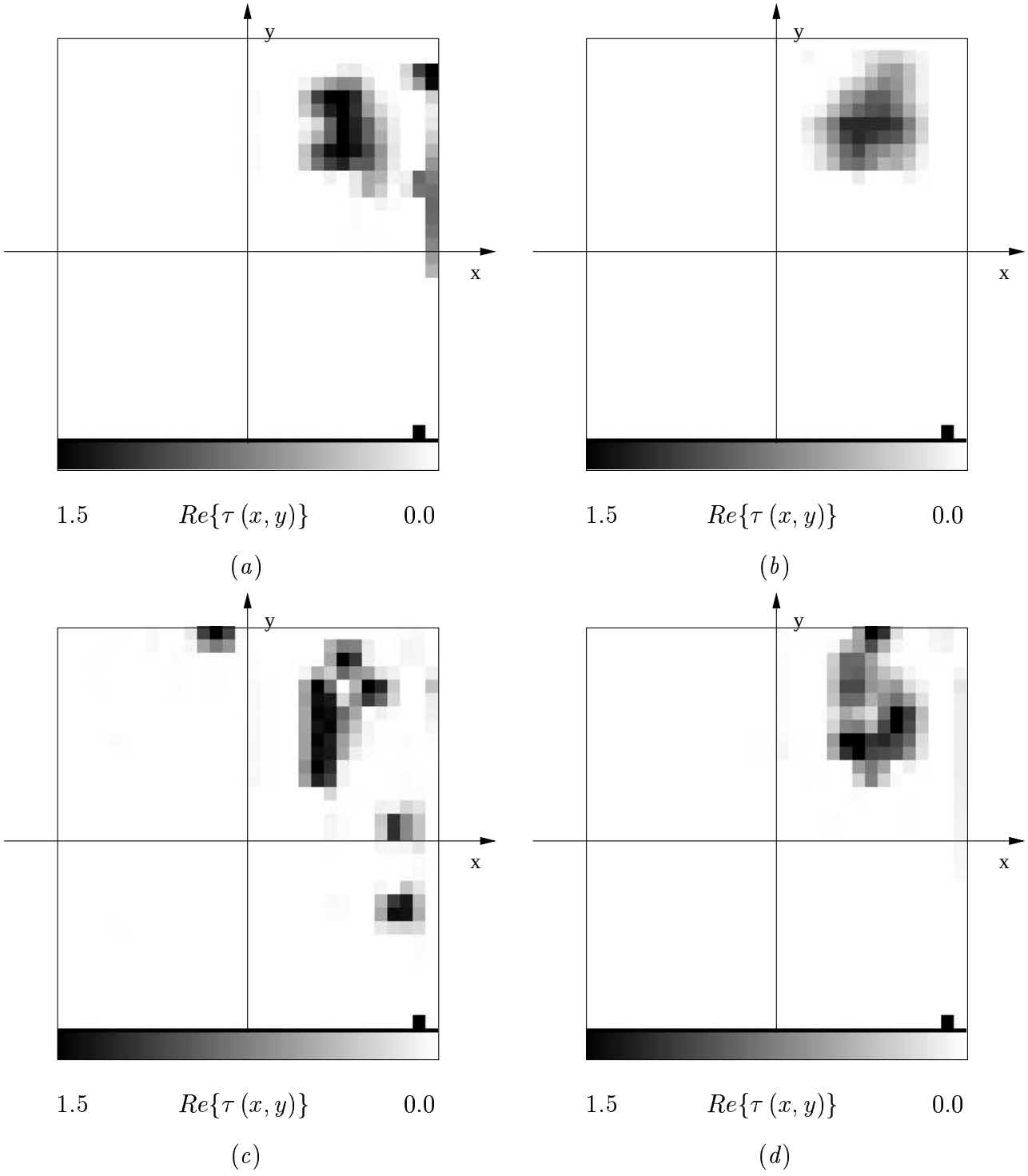

Fig. 5 - R. Azaro *et al.*, "An Innovative Fuzzy-Logic-Based Strategy ..."

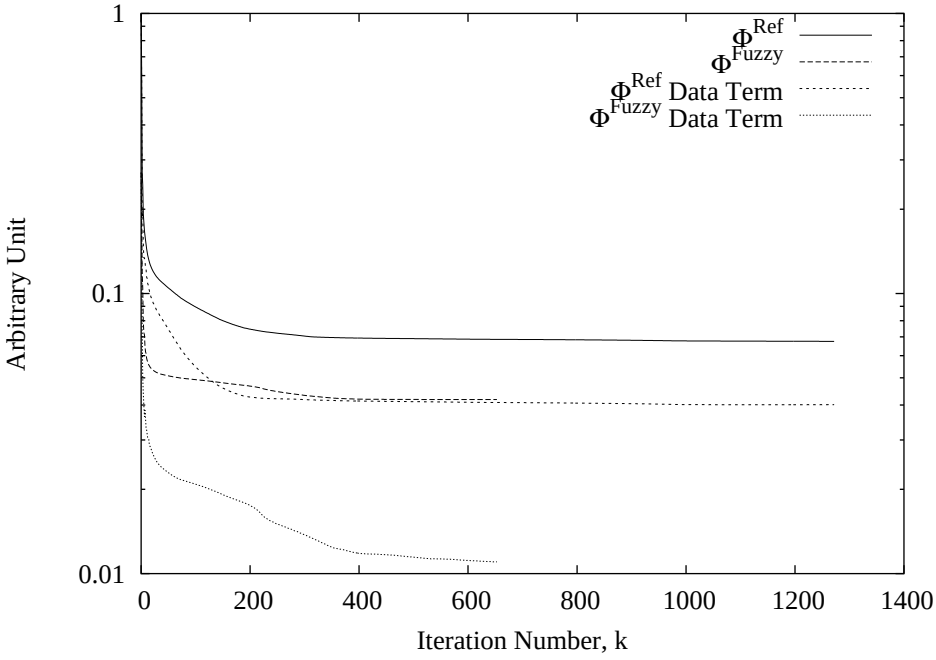

(a)

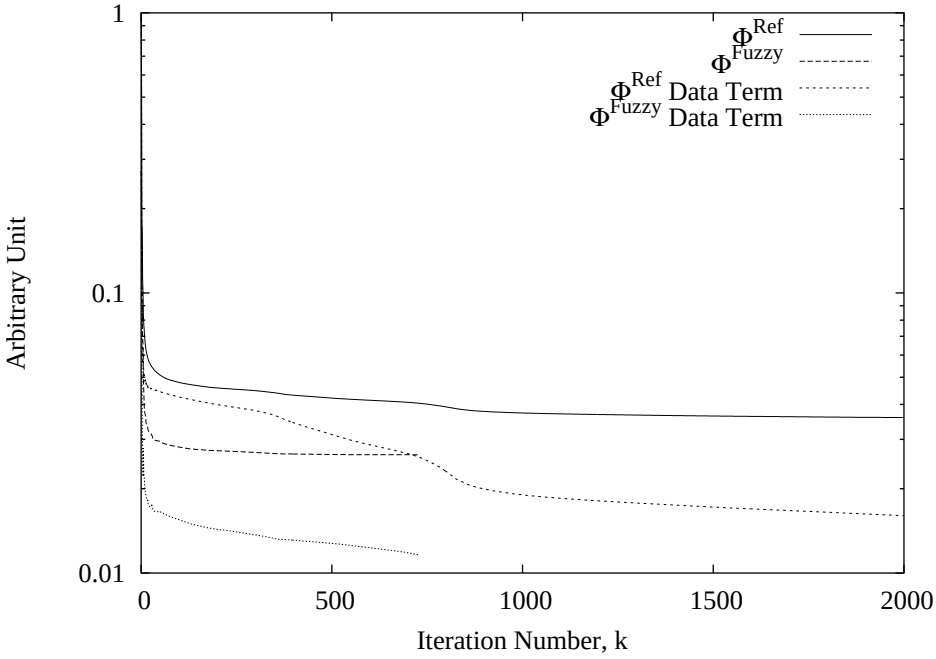

(b)

Fig. 6 - R. Azaro *et al.*, "An Innovative Fuzzy-Logic-Based Strategy ..."

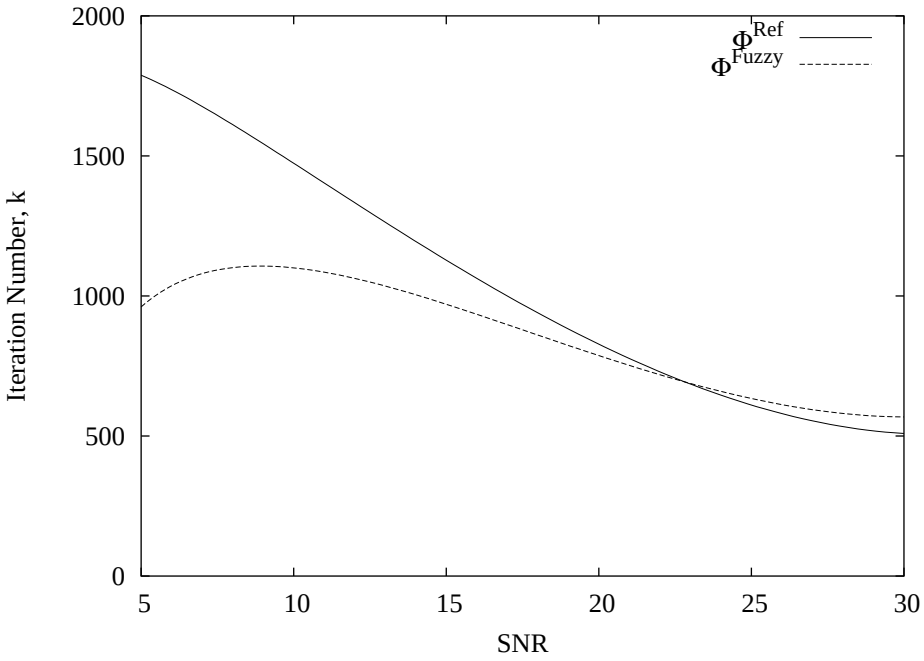

Fig. 7 - R. Azaro *et al.*, "An Innovative Fuzzy-Logic-Based Strategy ..."

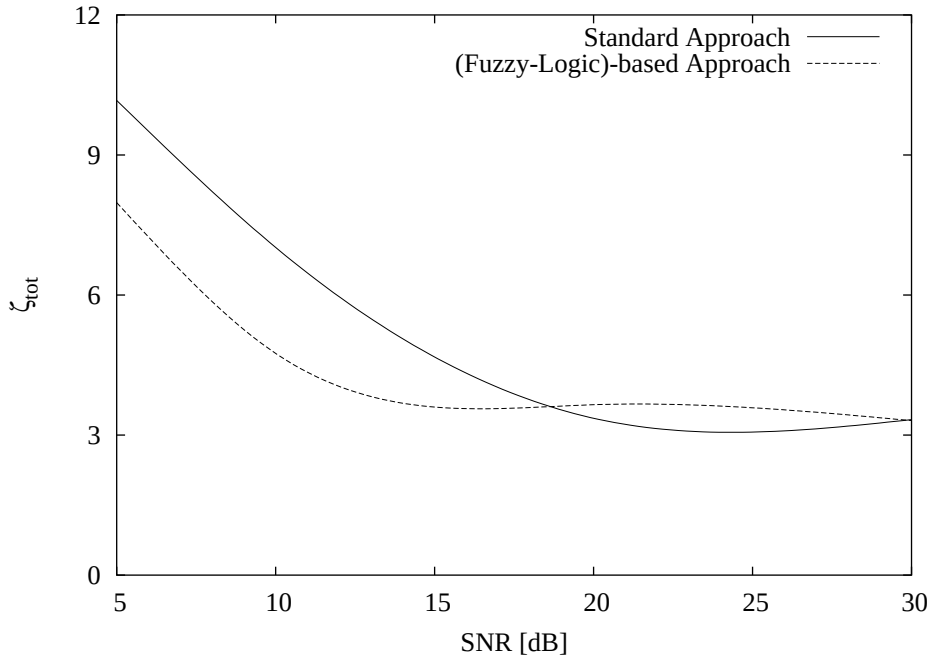

(a)

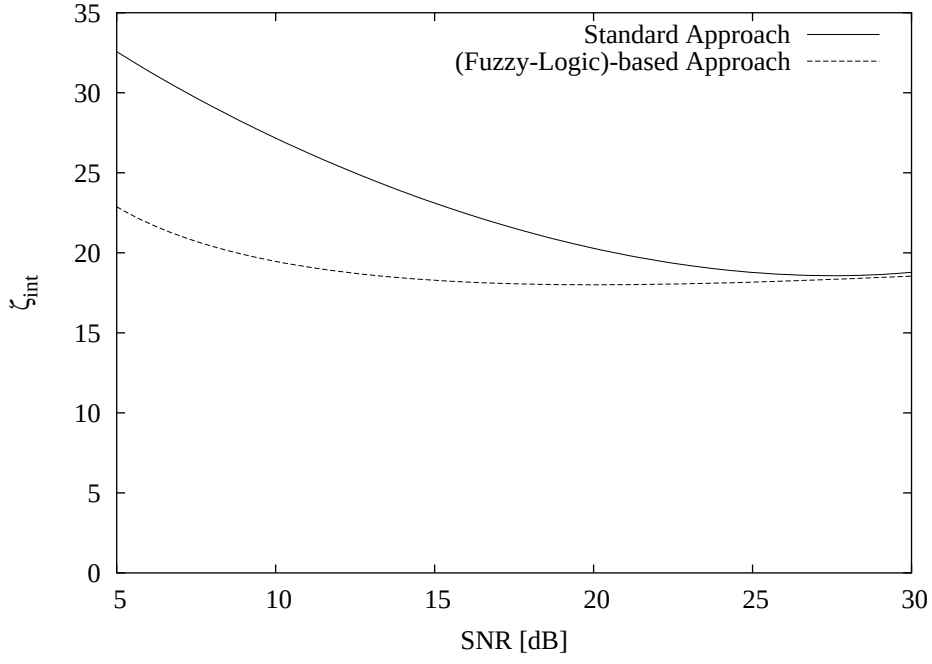

(b)

Fig. 8(I) - R. Azaro *et al.*, "An Innovative Fuzzy-Logic-Based Strategy ..."

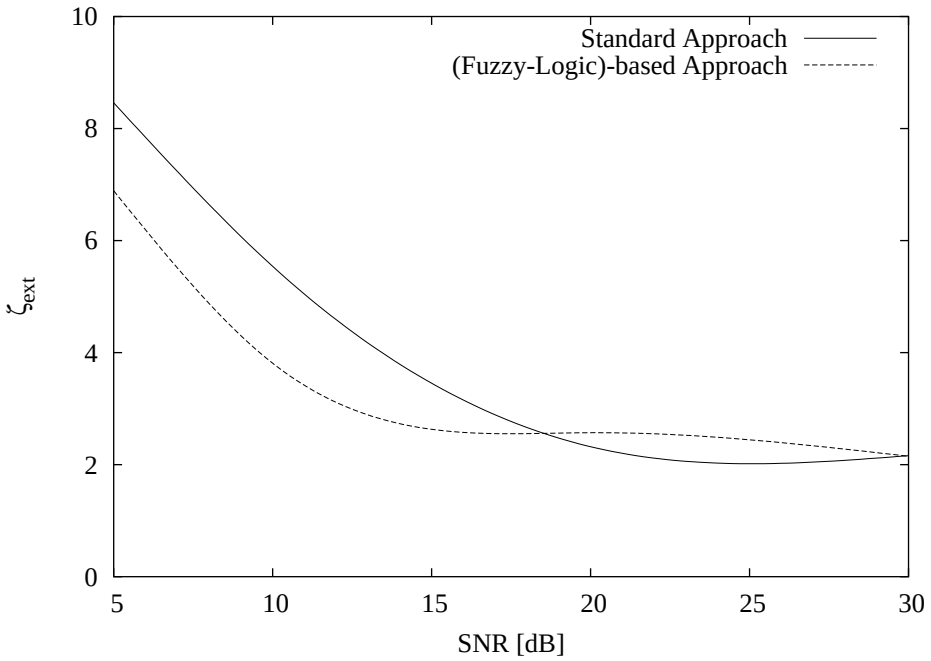

(c)

Fig. 8(*II*) - R. Azaro *et al.*, "An Innovative Fuzzy-Logic-Based Strategy ..."

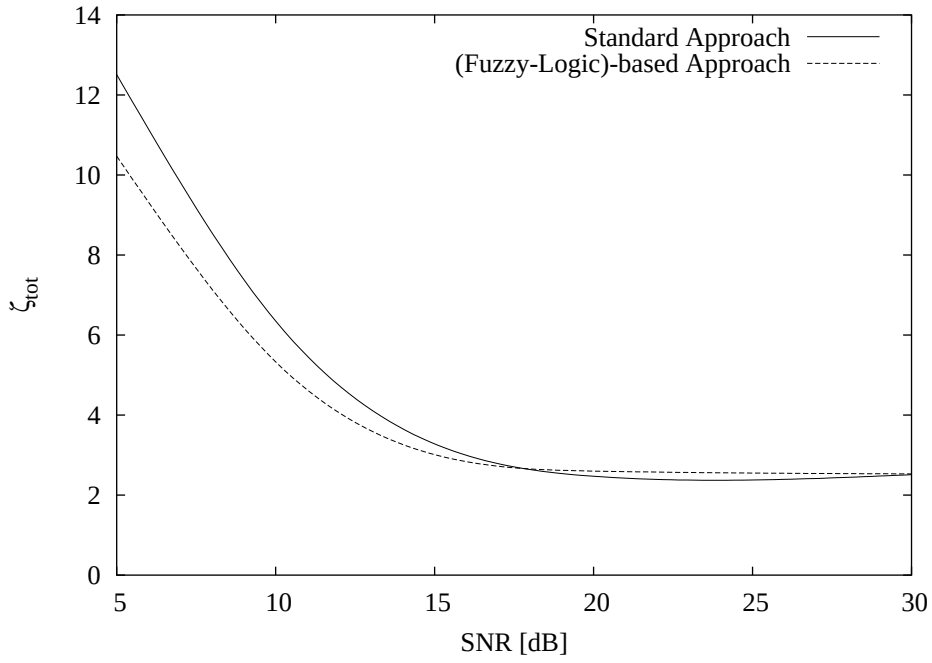

(a)

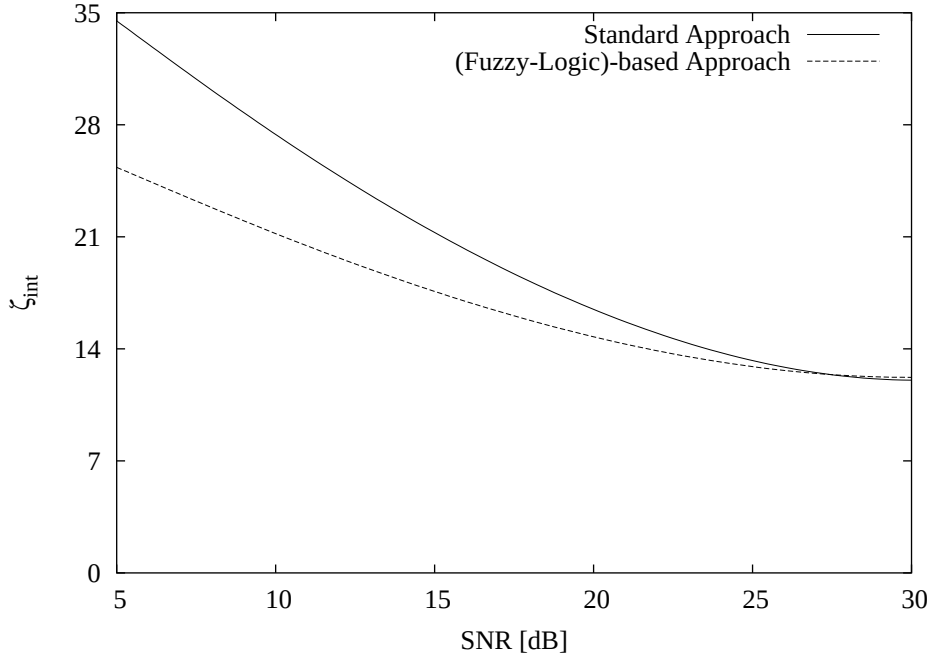

(b)

Fig. 9(I) - R. Azaro *et al.*, "An Innovative Fuzzy-Logic-Based Strategy ..."

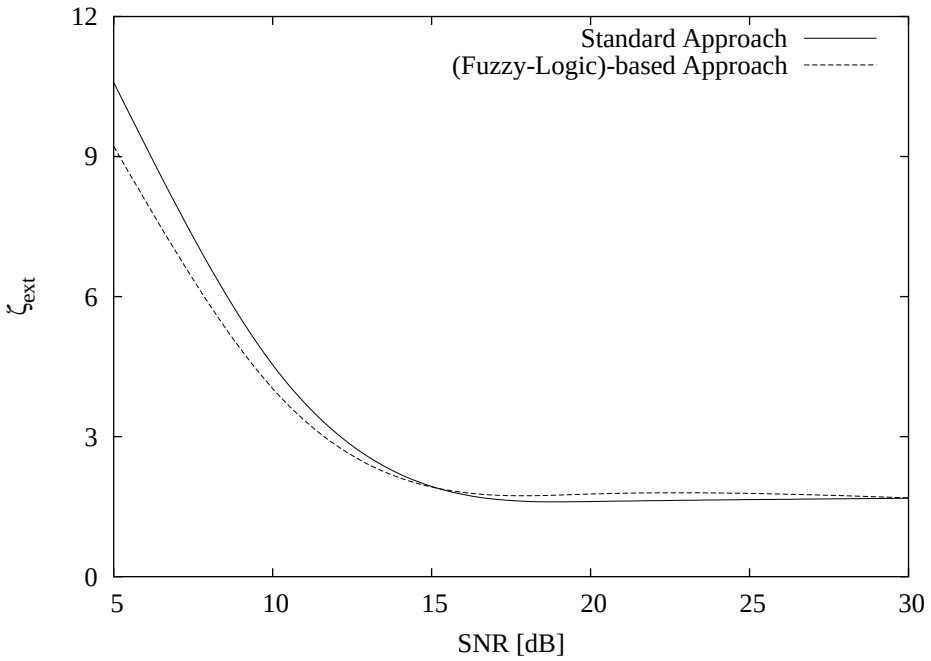

(c)

Fig. 9(*II*) - R. Azaro *et al.*, "An Innovative Fuzzy-Logic-Based Strategy ..."

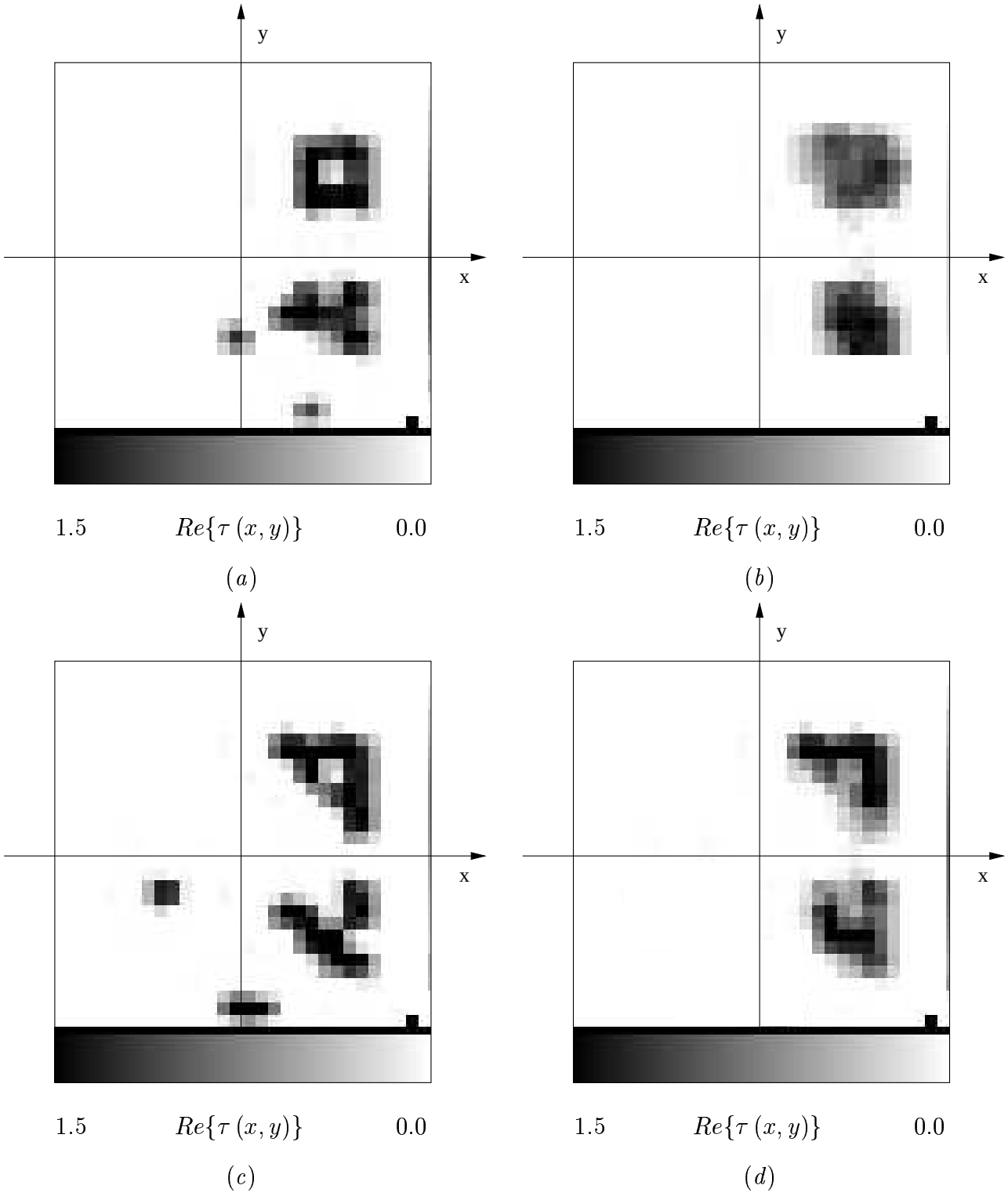

Fig. 10 - R. Azaro *et al.*, "An Innovative Fuzzy-Logic-Based Strategy ..."

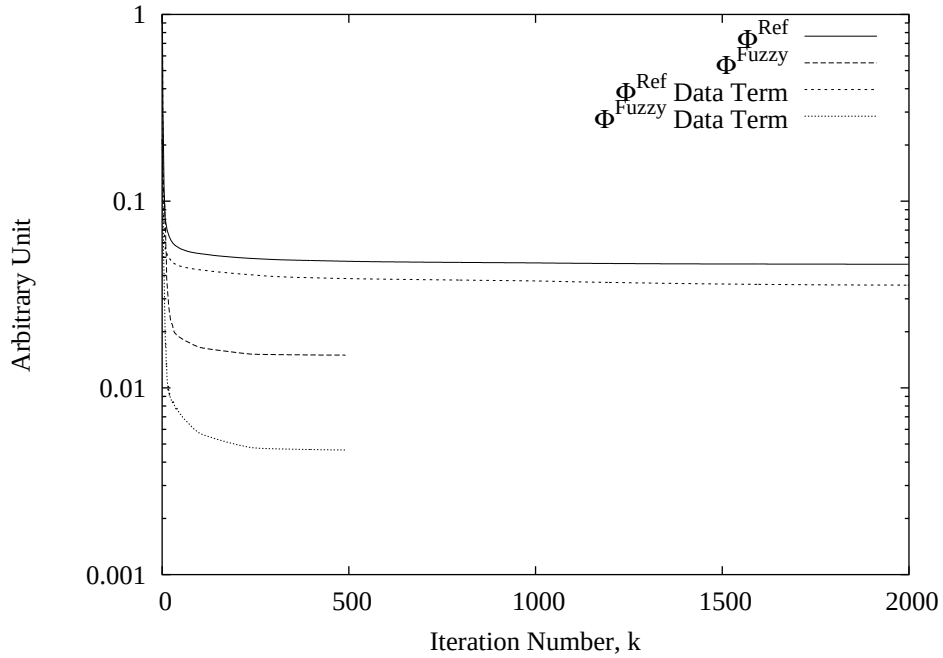

(a)

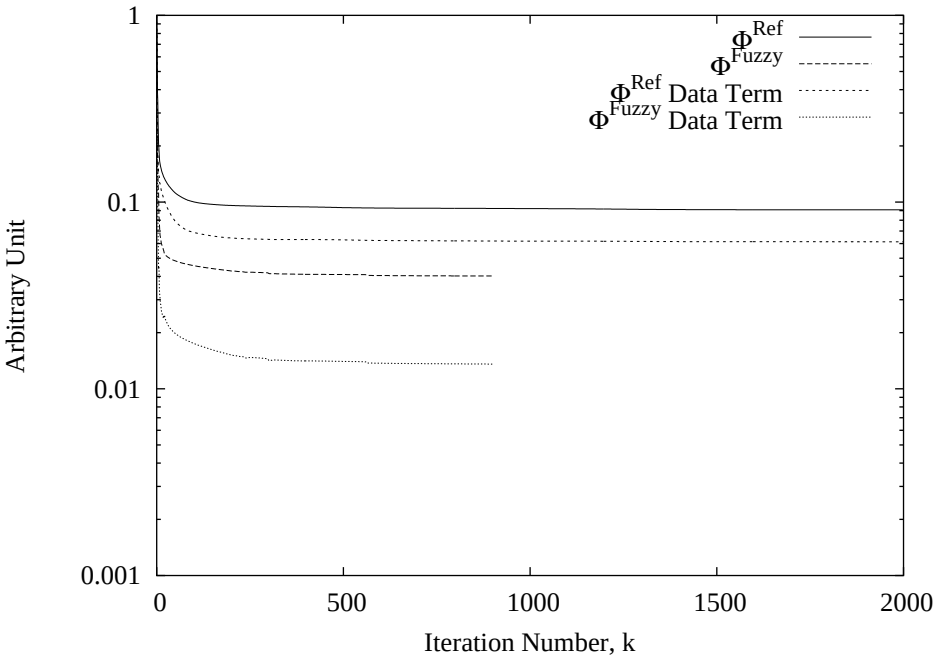

(b)

Fig. 11 - R. Azaro *et al.*, "An Innovative Fuzzy-Logic-Based Strategy ..."